

Supporting Information

Efficient Organic Light Emitting Diodes through a Hot Exciton Channel in Anthracene Derivatives

*Nidhi Sharma,^{a,b,‡} Michael Yin Wong,^{a,‡} David Hall,^{a,c} Eduard Spuling,^a Francisco Tenopala Carmona,^b Alberto Privitera,^d Graeme Copley,^a David B. Cordes,^a Alexandra M. Z. Slawin,^a Caroline Murawski,^{b,+} Malte C. Gather,^b David Beljonne,^c Yoann Olivier,^{*c,e} Ifor D. W. Samuel^{*b} and Eli Zysman-Colman^{*a}*

^a Organic Semiconductor Centre, EaStCHEM School of Chemistry, University of St Andrews, St Andrews, UK, KY16 9ST. E-mail: eli.zysman-colman@st-andrews.ac.uk; <http://www.zysman-colman.com>

^b Organic Semiconductor Centre, SUPA School of Physics and Astronomy, University of St Andrews, St Andrews, UK, KY16 9SS.

^c Laboratory for Chemistry of novel materials, University of Mons, Place du Parc 20, B-7000 Mons, Belgium.

^d Clarendon Laboratory, Department of Physics, University of Oxford, Parks Road, Oxford OX1 3PU, UK.

^e Unité de Chimie Physique Théorique et Structurale & Laboratoire de Physique du Solide, Namur Institute of Structured Matter, Université de Namur, Rue de Bruxelles, 61, 5000 Namur, Belgium.

Table of Contents

Experiment	Page Number
SI-1 Experimental Section	2
SI-2 Solvatochromic Experiments	8
SI-3. Photophysical Properties	10
SI-4 Time-resolved EPR measurements	11
SI-5. Electroluminescence Properties	12
SI-6. NMR Spectra	12
SI-7. HPLC Data	17
SI-8. Molecular Modelling	19
SI-9. Angle-resolved photoluminescence spectroscopy measurements	20
SI-10. High Resolution Mass Spectrometry (HRMS)	23

SI-1. Experimental Section.

General Synthetic Procedures. All the commercially available chemicals and reagent grade solvents were used as received. Air-sensitive reactions were performed using standard Schlenk techniques under a nitrogen atmosphere. Freshly distilled anhydrous THF was obtained from a Pure SolvTM solvent purification system (Innovative Technologies). Flash column chromatography was carried out using silica gel (Silica-P from Silicycle, 60 Å, 40-63 µm). Analytical thin-layer-chromatography (TLC) was performed with silica plates with aluminum backings (250 µm with F-254 indicator). TLC visualization was accomplished by 254/365 nm UV lamp. ¹H and ¹³C NMR spectra were recorded on Bruker Avance AVANCE II 400 MHz and 500 MHz spectrometers. Melting points were measured using open-ended capillaries on an electrothermal melting point apparatus IA9200 and are uncorrected. High-resolution mass spectrometry (HRMS) was performed by the EPSRC National Mass Spectrometry Service Centre (NMSSC), Swansea University and the Mass Spectrometry and Proteomics Facility of the University of St Andrews. Elemental analyses were performed by Mr. Stephen Boyer, London Metropolitan University.

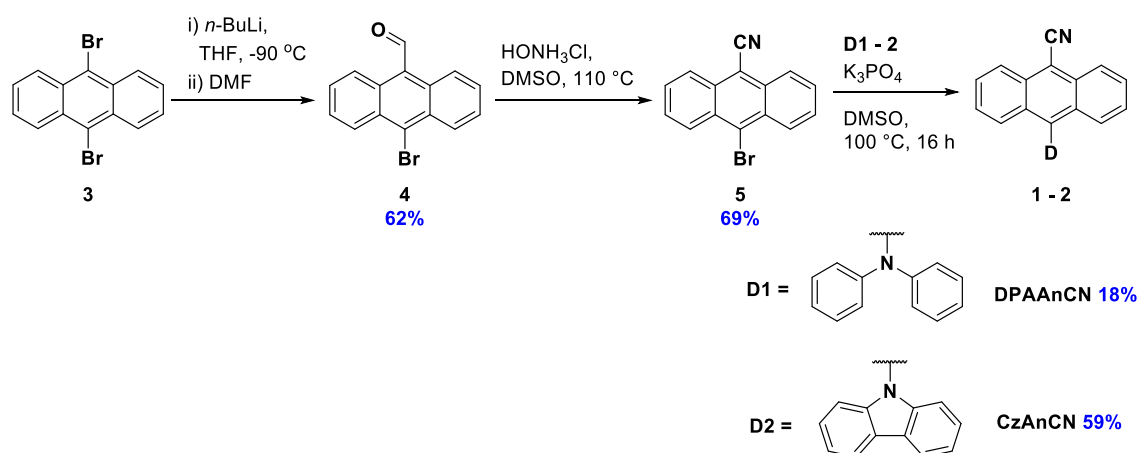
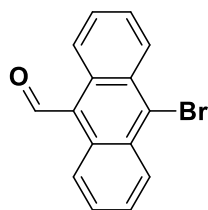


Figure S1. Synthesis of DPAAnCN and CzAnCN.

Preparation of 10-bromoanthracene-9-carbaldehyde (4)

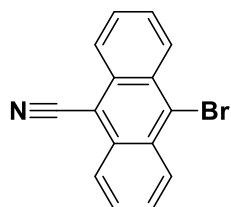


In a dried Schlenk flask, 9,10-dibromoanthracene (2.00 g, 5.95 mmol, 1.00 equiv.) was dissolved in dry THF (20 mL) and cooled to -90 °C under nitrogen. To this suspension was added dropwise *n*-BuLi (2.6 mL, 2.5 M, 6.55 mmol, 1.10 equiv.). The resulting red solution was stirred at -90 °C for 1h. Then the lithiate solution was warmed to 0 °C and dry DMF (875 μ L, 870 mg, 11.9 mmol, 2.00 equiv.) was added quickly and the mixture was stirred overnight (14 h) at room temperature. The mixture was quenched by addition of water and the organic phase extracted with ethyl acetate (3 \times 40 mL). The combined organic layers were washed with brine (50 mL), dried over Na₂SO₄ and the solvents removed under reduced pressure. The crude product was recrystallized from cold hexane to yield 1.05 g (62%, 3.70 mmol) of a yellow solid.

Yellow solid. **Yield:** 62%. **Mp:** 219 °C. **R_f:** 0.21 (ethyl acetate : hexanes = 20:1, silica). **¹H NMR (500 MHz, CDCl₃) δ (ppm):** 11.53 (s, 1H), 8.91 (d, *J* = 8.3 Hz, 2H), 8.70 (d, *J* = 8.4 Hz, 2H), 7.83 – 7.61 (m, 4H). **¹³C NMR (126 MHz, CDCl₃) δ (ppm):** 193.44, 132.08, 131.97, 130.43, 129.17, 129.06, 127.54, 125.87, 123.98. **HRMS (ESI): [M+H]⁺ Calculated:** (C₁₅H₁₀⁷⁹BrO) 284.9910; **Found:** 284.9912; **Calculated:** (C₁₅H₁₀⁸¹BrO) 286.9889, **Found:** 286.9892.

The analytical data matches that of the literature.¹

Preparation of 10-bromoanthracene-9-carbonitrile (5)



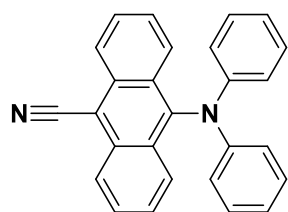
In a dried flask, 10-bromoanthracene-9-carbaldehyde (900 mg, 3.16 mmol, 1.00 equiv.) and hydroxylammonium chloride (877 mg, 12.6 mmol, 4.00 equiv.) were dissolved in DMSO (20 mL). The reaction mixture was stirred at 110 °C for 2 h. The reaction mixture was cooled to room temperature, diluted with ethyl acetate (60 mL) and washed with brine (3 \times 50 mL) to remove all the DMSO. The organic layer was dried over Na₂SO₄ and the solvent removed under reduced pressure. The

crude product was recrystallized from *isopropanol* to yield 621 mg (69%, 2.20 mmol) of a yellow solid.

Yellow solid. **Yield:** 69%. **Mp:** 264 °C. **R_f:** 0.30 (ethyl acetate : hexanes = 20:1, silica). **¹H NMR (500 MHz, CDCl₃) δ (ppm):** 8.59 (d, *J* = 8.7 Hz, 2H), 8.43 (d, *J* = 8.7 Hz, 2H), 7.76 – 7.68 (m, 4H). **¹³C NMR (126 MHz, CDCl₃) δ (ppm):** 133.50, 130.47, 130.17, 129.33, 128.82, 128.21, 125.91, 117.09, 106.47. **HRMS (ASAP): [M]⁺ Calculated:** (C₁₅H₉⁷⁹BrN) 281.9913; **Found** 281.9916; **Calculated:** (C₁₅H₉⁸¹BrN) 283.9892; **Found** 283.9895.

The analytical data matches that of the literature.¹⁻²

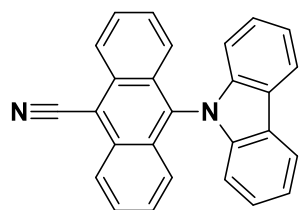
Preparation of 9-cyano-10-diphenylaminoanthracene, **DPAAnCN**, (**1**)



In a dried flask, 10-bromoanthracene-9-carbonitrile (220 mg, 0.780 mmol, 1.00 equiv.), diphenylamine (296 mg, 2.34 mmol, 3.00 equiv.) and K₃PO₄ (828 mg, 3.90 mmol, 5.00 equiv.) were dissolved in DMSO (20 mL) and then stirred at 100 °C for 16 h. The reaction mixture was then diluted with ethyl acetate (60 mL) and washed with brine (3 × 50 mL) to remove all the DMSO. The organic layer was dried over Na₂SO₄ and the solvent removed under reduced pressure. The crude product was purified by column chromatography (hexane/ethyl acetate; 20/1) and subsequently recrystallized in methanol to yield 53 mg (18%, 0.143 mmol) of an orange solid.

Orange solid. **Yield:** 18%. **Mp:** 233 °C. **R_f:** 0.36 (ethyl acetate:hexanes; 1:10, silica). **¹H NMR (300 MHz, CDCl₃) δ (ppm):** 8.50 (d, *J* = 8.7 Hz, 2 H), 8.20 (d, *J* = 8.8 Hz, 2 H), 7.71 – 7.66 (m, 2 H), 7.51 – 7.45 (m, 2 H), 7.22 – 7.16 (m, 4 H), 7.05 – 7.02 (m, 4 H), 6.97 – 6.91 (m, 2 H). **¹³C NMR (76 MHz, CDCl₃) δ (ppm):** 147.66, 143.66, 134.83, 130.27, 129.60, 129.00, 127.62, 126.25, 125.53, 122.20, 120.82, 117.40, 105.64. **HRMS (ESI): [M+H]⁺ Calculated:** (C₂₇H₁₉N₂) 371.1543; **Found:** 371.1540. **Anal. Calcd. for C₂₇H₁₈N₂:** C 87.54, H 4.90, N 7.56; **Found:** C 87.44, H 5.03, N 7.45.

Preparation of 9-(N-carbazolyl)-10-cyanoanthracene, CzAnCN, (2)



In a dried flask, 10-bromoanthracene-9-carbonitrile (420 mg, 1.50 mmol, 1.00 equiv.), carbazole (502 mg, 3.00 mmol, 2.00 equiv.) and K_3PO_4 (850 mg, 4.00 mmol, 2.66 equiv.) were dissolved in DMSO (20 mL) and then stirred at 100 °C for 16 h. The reaction mixture was then diluted with ethyl acetate (60 mL) and washed with brine (3×50 mL) to remove all the DMSO. The organic layer was dried over Na_2SO_4 and the solvent was removed under reduced pressure. The crude product was purified by column chromatography (hexane/ethyl acetate; 20/1) and subsequently washed with pentane to yield 323 mg (59%, 0.877 mmol) of a green solid.

Green solid. **Yield:** 59%. **Mp:** 252 °C. **R_f:** 0.43 (ethyl acetate:hexanes; 1:20, silica). **¹H NMR (400 MHz, CD₂Cl₂) δ (ppm):** 8.61 (d, $J = 8.7$ Hz, 2 H), 8.31 (dd, $J = 7.7, 0.9$ Hz, 2 H), 7.80 – 7.76 (m, 2 H), 7.45 – 7.41 (m, 2 H), 7.37 – 7.27 (m, 6 H), 6.69 (d, $J = 7.9$ Hz, 2 H). **¹³C NMR (100 MHz, CD₂Cl₂) δ (ppm):** 143.06, 135.55, 134.50, 129.98, 129.92, 128.48, 126.95, 126.52, 124.89, 123.95, 121.16, 121.03, 117.29, 110.58, 108.09. **HRMS (ESI): [M+H]⁺ Calculated:** (C₂₇H₁₇N₂) 369.1386, **Found:** 369.1389. **Anal. Calcd. for C₂₇H₁₆N₂:** C 88.02, H 4.38, N 7.60; **Found:** C 87.90, H, 4.26, N, 7.60.

Photophysical measurements. Optically dilute solutions of concentrations in the order of 10^{-5} or 10^{-6} M were prepared in HPLC grade solvent for absorption and emission analysis. Absorption spectra were recorded at room temperature on a Shimadzu UV-1800 double beam spectrophotometer. Molar absorptivity values were determined from at least four solutions followed by linear regression analysis. Aerated solutions were bubbled with compressed air for 5 minutes whereas degassed solutions were prepared via five freeze-pump-thaw cycles prior to emission analysis using an in-house adapted fluorescence cuvette, itself purchased from Starna. Steady-state emission and excitation spectra and time-resolved emission spectra were recorded at 298 K using an Edinburgh Instruments F980 fluorimeter. Samples were excited at 360 nm

for steady-state measurements and at 378 nm for time-resolved measurements. Photoluminescence quantum yields for solutions were determined using the optically dilute method³ in which four sample solutions with absorbance at 360 nm being ca. 0.10, 0.080, 0.060 and 0.040 were used. Their emission intensities were compared with those of a reference, quinine sulfate, whose quantum yield (Φ_r) in 1 N H₂SO₄ was determined to be 54.6% using absolute method.⁴ The quantum yield of the sample, Φ_{PL} , can be determined by the equation $\Phi_{PL} = \Phi_r * \frac{A_r}{A_s} * \frac{I_s}{I_r} * \frac{n_s^2}{n_r^2}$, where A stands for the absorbance at the excitation wavelength (λ_{exc} : 360 nm), I is the integrated area under the corrected emission curve and n is the refractive index of the solvent with the subscripts “s” and “r” representing sample and reference respectively. To prepare the 10 wt% doped films of emitters in a host matrix, 95% w/w (95 mg) of host was dissolved in 1 mL of solvent and to this, 5% w/w (5 mg) of emitter was added. Thin films were then spin-coated on a quartz substrate using a spin speed of 1500 rpm for 60 s to give a thickness of ~80 nm. An integrating sphere (Hamamatsu, C9920-02) was employed for quantum yield measurements for thin film samples.

Electrochemistry measurements. Cyclic Voltammetry (CV) analysis was performed on an Electrochemical Analyzer potentiostat model 600D from CH Instruments. Samples were prepared as MeCN solutions, which were degassed by sparging with MeCN-saturated nitrogen gas for 15 minutes prior to measurements. All measurements were performed in 0.1 M MeCN solution of tetrabutylammonium hexafluorophosphate, which was used as the supporting electrolyte. An Ag/Ag⁺ electrode was used as the reference electrode while a platinum electrode and a platinum wire were used as the working electrode and counter electrode, respectively. The redox potentials are reported relative to a saturated calomel electrode (SCE) with a ferrocene/ferrocenium (Fc/Fc⁺) redox couple as the internal standard (0.38 V vs SCE).⁵

X-Ray crystallography. X-ray diffraction data for both compounds **DPAAnCN** and **CzAnCN** were collected at 173 K using a Rigaku FR-X Ultrahigh brilliance Microfocus RA generator/confocal optics with XtaLAB P200 diffractometer [Mo K α radiation ($\lambda = 0.71075$ Å)]. Intensity data were collected using ω -steps accumulating area detector images spanning at least a hemisphere of reciprocal space. Data were collected and processed (including correction for Lorentz polarization and absorption) using CrystalClear.⁶ Structures were solved by direct methods (SIR2011)⁷ and refined by full-matrix least-squares against F² (SHELXL-2018/3).⁸ Non-hydrogen atoms were refined anisotropically, and hydrogen atoms were refined using a riding model. All calculations were performed using the CrystalStructure⁹ interface. Selected crystallographic data are presented in Table S1. CCDC 1960941-1960942 contains the supplementary crystallographic data for this paper. The data can be obtained free of charge from The Cambridge Crystallographic Data Centre via www.ccdc.cam.ac.uk/structures.

Time-resolved EPR measurements. Time-resolved EPR (TREPR) spectra were recorded on a Bruker Eleksys E680 X-band spectrometer, equipped with a nitrogen gas-flow cryostat for sample temperature control. The sample temperature was maintained with an Oxford Instruments CF9350 cryostat and controlled with an Oxford Instruments ITC503.

TREPR experiments were performed recording the EPR signal after a short laser pulse produced by an Oportek Opolette Opto-parametric Oscillator (OPO) tunable laser (20 Hz repetition rate, E/pulse \approx 3 mJ, $\lambda = 410$ -700 nm). The TREPR signal was recorded through a Bruker SpecJet transient recorder. The spectra were acquired with 2 mW microwave power and averaging 300 transient signals at each field position. TREPR spectral simulations were carried out using the Matlab toolbox Easyspin.

TREPR measurements were performed on **DPAAnCN** and **CzAnCN** dissolved in toluene solution (10 mg/mL). The solutions were poured inside quartz EPR tubes (inner diameter = 3 mm), which were sealed under vacuum after several freeze-pump-thaw cycles.

Table S1. Selected crystallographic data.

	DPAAAnCN	CzAnCN
empirical formula	C ₂₇ H ₁₈ N ₂	C ₂₇ H ₁₆ N ₂
fw	370.45	368.44
crystal description	Orange prism	Yellow prism
crystal size [mm ³]	0.18×0.10×0.08	0.12×0.07×0.04
space group	<i>P</i> 2 ₁ / <i>n</i>	<i>P</i> 2 ₁ / <i>c</i>
<i>a</i> [Å]	10.4404(17)	14.483(3)
<i>b</i> [Å]	13.660(2)	9.4676(17)
<i>c</i> [Å]	13.573(2)	14.148(2)
β [°]	96.071(4)	108.793(5)
vol [Å ³]	1924.9(5)	1836.5(6)
<i>Z</i>	4	4
ρ (calc) [g/cm ³]	1.278	1.332
μ [mm ⁻¹]	0.075	0.078
F(000)	776	768
reflections collected	23037	21587
independent reflections (<i>R</i> _{int})	3514 (0.0399)	3360 (0.0679)
data/restraints/parameters	3514/0/262	3360/0/262
GOF on <i>F</i> ²	1.035	0.917
<i>R</i> _I [<i>I</i> > 2σ(<i>I</i>)]	0.0406	0.0392
<i>wR</i> ₂ (all data)	0.1084	0.0825
largest diff. peak/hole [e/Å ³]	0.19, -0.22	0.15, -0.17

SI-2. Solvatochromic Experiments

Lippert-Mataga Model.

The Lippert-Mataga model, which relates the Stokes shift to the solvent polarity factor *f*, can be estimated from the following equation:¹⁰

$$hc(v_{abs} - v_{PL}) = hc(v_{abs}^0 - v_{PL}^0) - \frac{2(\mu_e - \mu_g)^2}{a^3} f(\epsilon, n),$$

where *f* is the orientational polarizability of the solvent; *v_a* – *v_f* corresponds to the Stokes shifts when *f* is zero; μ_e is the excited-state dipole moment; μ_g is the ground-state dipole moment; *a* is the solvent cavity (Onsager) radius derived from Avogadro's number (*N*), the molecular weight (*M*), and the density (*d* = 1.0 g/cm³); ϵ and *n* are the solvent dielectric and

the solvent refractive index, respectively; $f(\varepsilon, n)$ and a can be calculated, respectively, as follows:

$$f(\varepsilon, n) = \frac{\varepsilon - 1}{2\varepsilon + 1} - \frac{n^2 - 1}{2n^2 + 1}, a = \left(\frac{3M}{4N\pi d}\right)^{1/3}$$

The detailed data are shown in Table S2.

Table S2. Detailed solvatochromic investigations of absorption and emission.

Solvent	ε	n	$f(\varepsilon, n)$	DPAAnCN			CzAnCN		
				λ_{abs}	λ_{PL}	$\nu_{\text{abs}} - \nu_{\text{PL}}$	λ_{abs}	λ_{PL}	$\nu_{\text{abs}} - \nu_{\text{PL}}$
				nm	nm	cm ⁻¹	nm	nm	cm ⁻¹
Hexane	1.9	1.375	0.0012	468	515	1950.04	428	453	1289.43
Toluene	2.38	1.494	0.014	478	559	3031.41	436	495	2733.76
Triethylamine	2.42	1.401	0.047	475	535	2361.04	430	480	2422.48
Dibutylether	3.1	1.399	0.096	476	545	2659.78	430	485	2637.25
Diisopropylether	3.88	1.367	0.145	471	550	3049.60	435	494	3012.90
Ethylacetate	6.02	1.372	0.199	472	590	4237.29	436	530	4120.58
THF	7.58	1.407	0.209	475	600	4385.96	429	538	4348.42
Chloroform	4.81	1.445	0.148	478	580	3679.12	430	520	4079.25
Methanol	32.7	1.328	0.308	467	631	5565.41	430	572	5773.30
Acetone	20.7	1.371	0.279	465	625	5505.37	430	560	5398.67
Acetonitrile	37.5	1.344	0.305	467	638	5739.30	430	581	6044.11

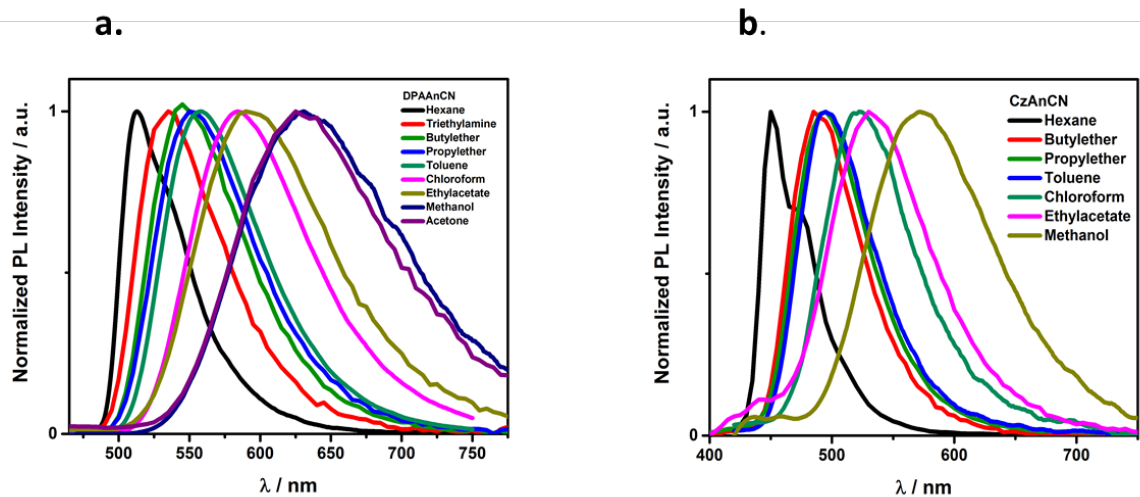


Figure S1. Solvatochromic PL spectra of a) **DPAAAnCN** and b) **CzAnCN**.

SI-3. Photophysical Properties.

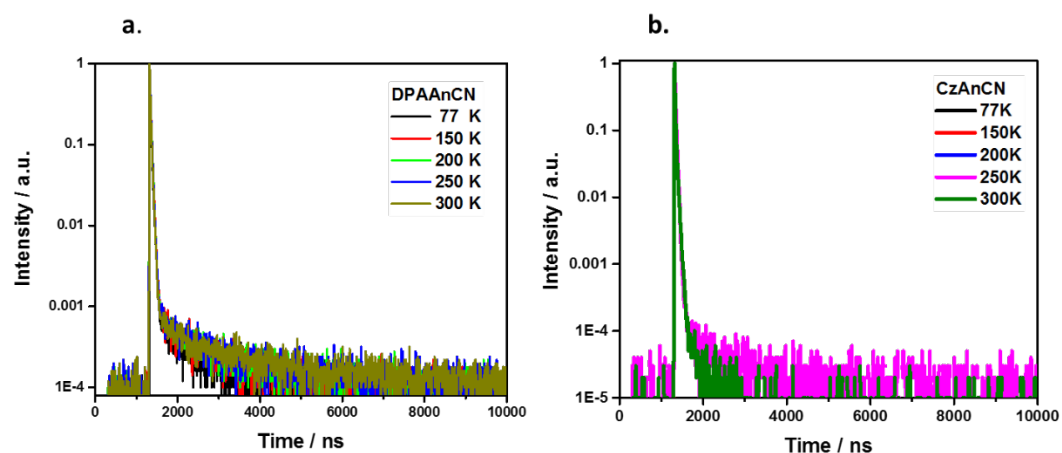


Figure S2. Variable temperature normalized transient PL decay spectra of a) **DPAAAnCN** and b) **CzAnCN** in 10 wt% doped films in mCP (at λ_{exc} 378 nm).

SI-4. Time-resolved EPR measurements

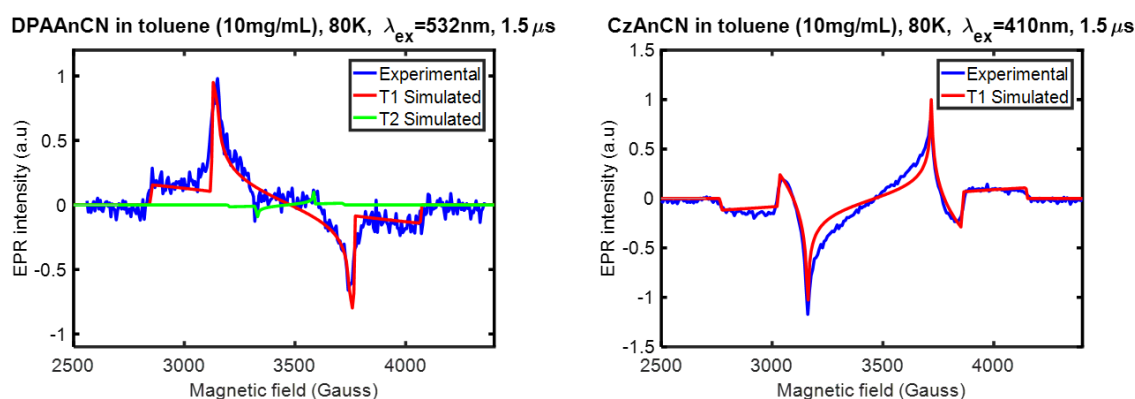


Figure S3. TREPR spectra at 80 K (blue line) of **DPAAAnCN** and **CzAnCN** in toluene solution recorded 1.5 μ s after a 532 nm and 410 nm laser pulse, respectively. From the best-fit spectral simulations of T₁ (red line) and T₂ (green line), the ZFS parameters reported in Table S_X were obtained.

Table S3. Values obtained from the best-fit spectral simulations of TREPR spectra reported in Figure S3. The parameters D and E are the zero-field splitting parameters defining the dipolar interaction between the two unpaired electrons of the triplet state. The populations p_x , p_y and p_z represent the values of the non-equilibrium populations of the three triplet sublevels populated by intersystem crossing. Given the low intensity of triplet T₂, the approximation E=0 has been adopted for the simulation. Despite this approximation is not strictly correct, the obtained D value can still provide a good qualitative estimate of T₂ triplet delocalization.

	[D E] Gauss	p_x, p_y, p_z
T₁ (DPAAAnCN)	[610 10]	0.44, 0.33, 0.44
T₂ (DPAAAnCN)	[260 0]	0.22, 0.33, 0.44
T₁ (CzAnCN)	[690 45]	0.25, 0.51, 0.24

SI-5. Electroluminescence Properties.

Table S4. Absolute Φ_{PL} measurements of vacuum deposited films of **DPAAnCN** and **CzAnCN** as a function of doping concentrations.

mCP : DPAAnCN	Φ_{PL} / % Nitrogen [Air]	mCP : CzAnCN	Φ_{PL} / % Nitrogen [Air]
5 wt %	54 [54]	5 wt %	32 [31]
7 wt%	53 [53]	7 wt%	35 [35]
10 wt%	56 [56]	10 wt%	45 [44]
15 wt%	44 [43]	15 wt%	40 [38]

SI-6. NMR Spectra.

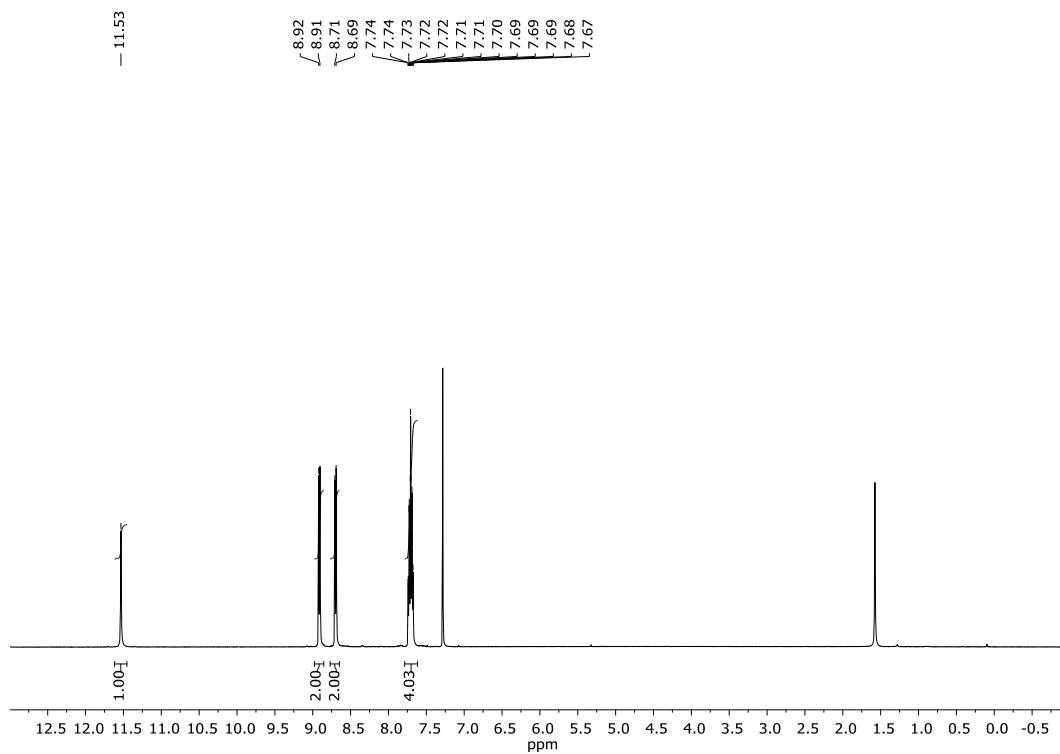


Figure S4. ^1H NMR spectrum of 10-bromoanthracene-9-carbaldehyde (**4**).

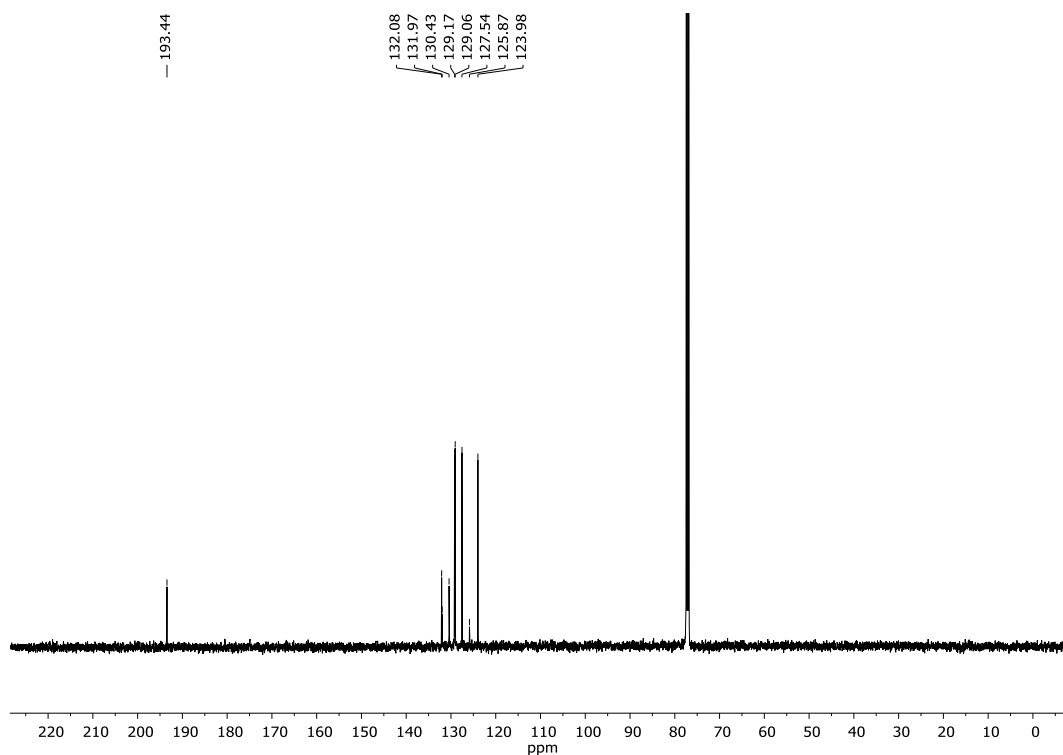


Figure S5. ^{13}C NMR spectrum of 10-bromoanthracene-9-carbaldehyde (**4**).

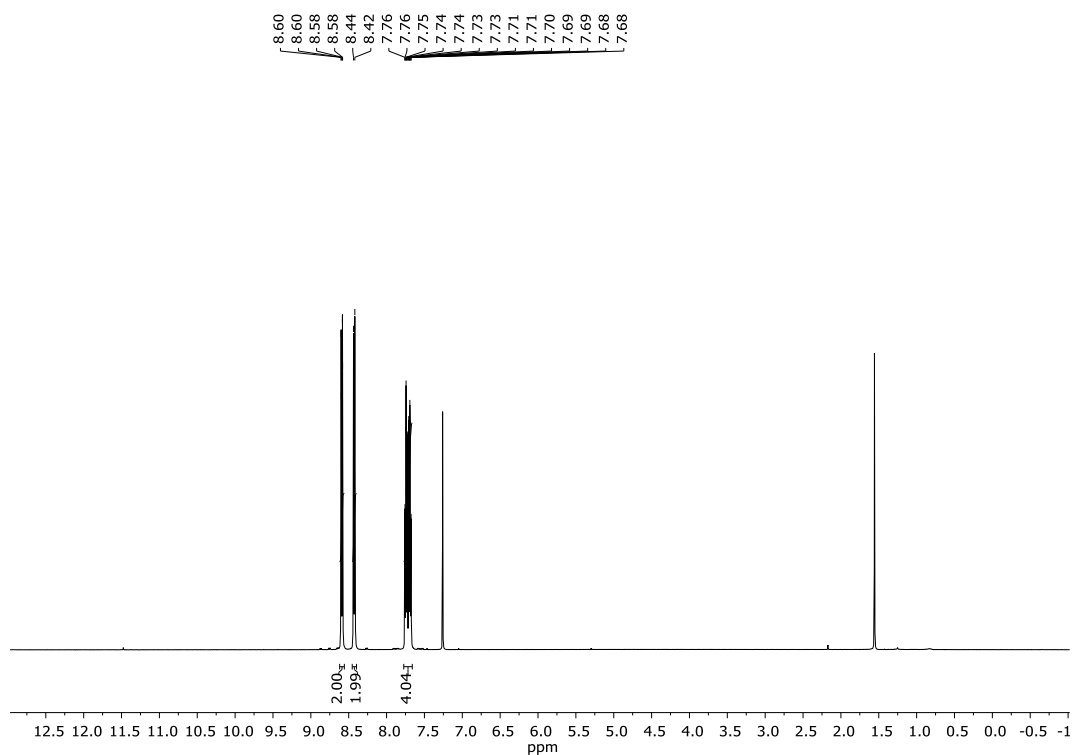


Figure S6. ^1H NMR spectrum of 10-bromoanthracene-9-carbonitrile (**5**).

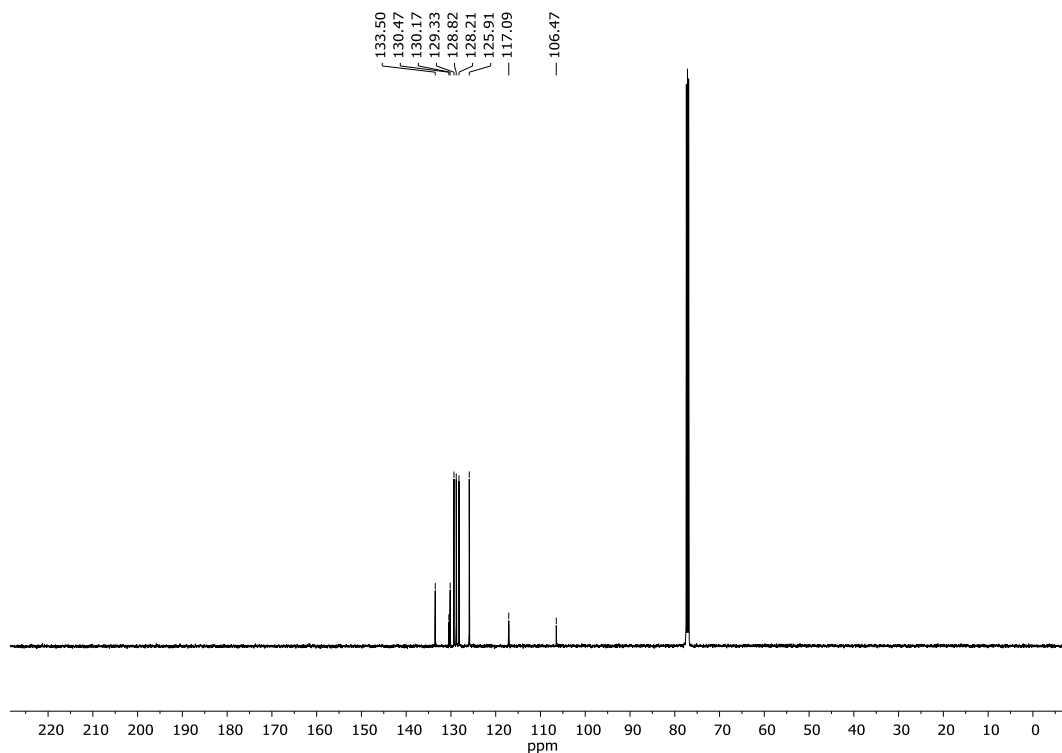


Figure S7. ^{13}C NMR spectrum of 10-bromoanthracene-9-carbonitrile (**5**).

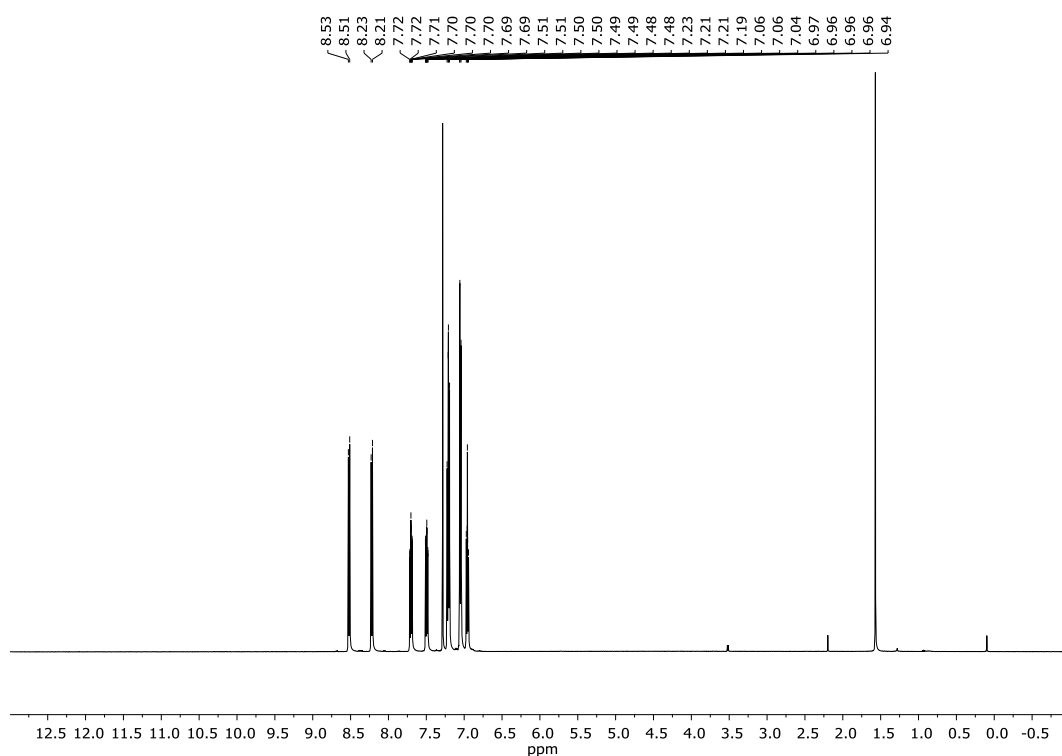


Figure S8. ^1H NMR spectrum of DPAAnCN.

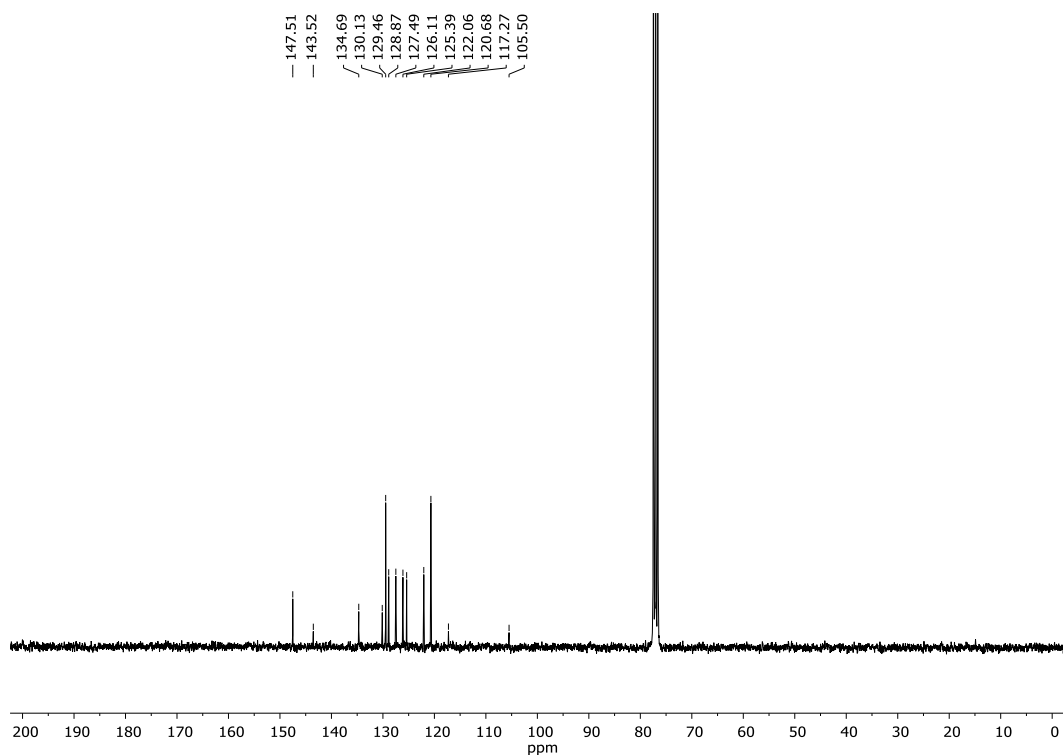


Figure S9. ^{13}C NMR spectrum of DPAAncN.

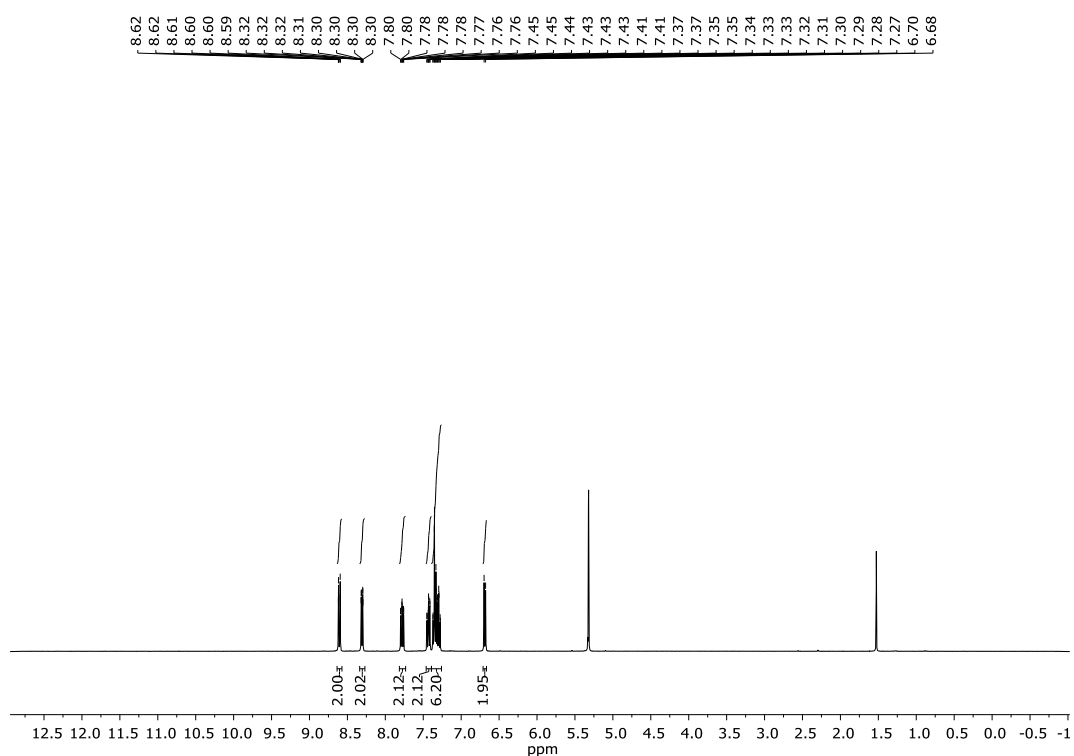


Figure S10. ^1H NMR spectrum of CzAnCN.

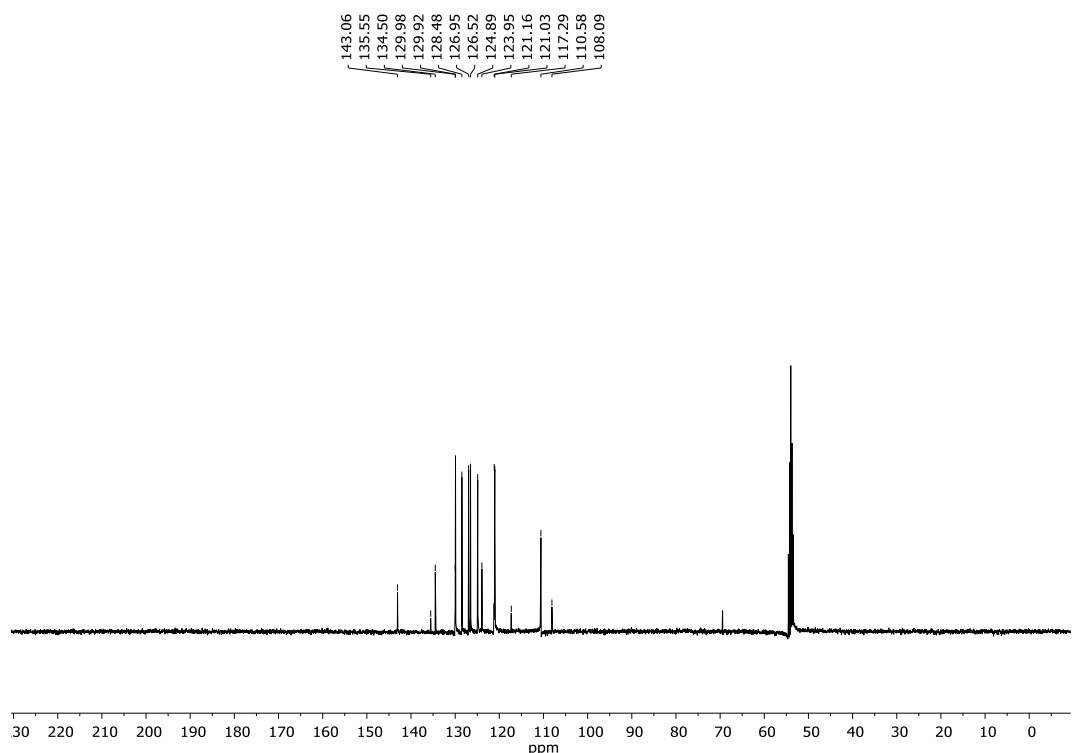
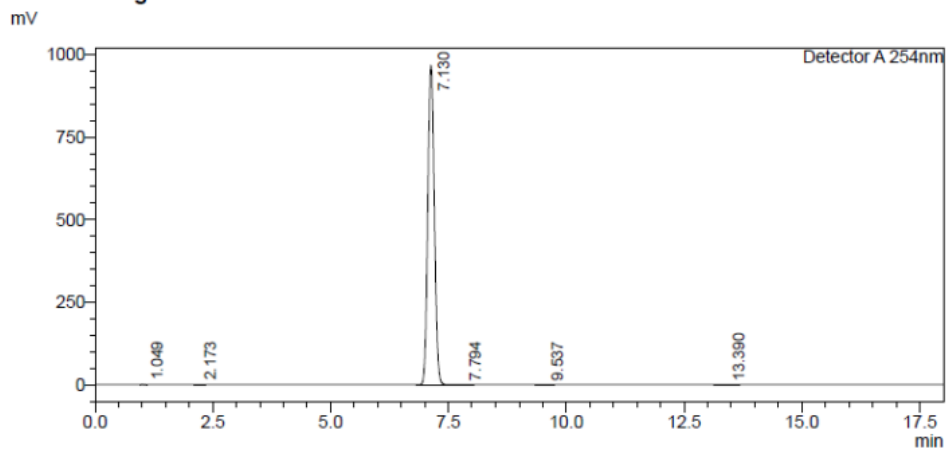


Figure S11. ^{13}C NMR spectrum of CzAnCN.

SI-7. HPLC Data.

Sample Name : DPAAAnCN
 Sample ID : ES025
 Method Filename : ACN80_H2O20.lcm
 Batch Filename : Anthracene_Emitters_ACN80_H2O20.lcb
 Vial # : 1-11
 Injection Volume : 10 uL
 Date Acquired : 11/11/2019 18:34:06
 Date Processed : 11/11/2019 18:52:09
 Sample Type : Unknown
 Acquired by : System Administrator
 Processed by : System Administrator

<Chromatogram>



<Peak Table>

Detector A 254nm

Peak#	Ret. Time	Area	Height	Area%	Area/Height	Width at 5% Height
1	1.049	3144	723	0.034	4.349	0.106
2	2.173	2277	417	0.025	5.458	--
3	7.130	9272374	966245	99.882	9.596	0.311
4	7.794	1748	201	0.019	8.712	0.274
5	9.537	1036	96	0.011	10.819	0.352
6	13.390	2786	189	0.030	14.772	0.478
Total		9283366	967870	100.000		

Figure S12. HPLC run of CzAnCN.

SI-8. Molecular Modeling.

Computational methodology

All ground state optimizations have been carried out at the Density Functional Theory (DFT) level with Gaussian09¹¹ using the PBE0 functional and the 6-31G(d,p) basis set. Excited state calculations have been performed at Time-Dependent DFT (TD-DFT) within the Tamm-Dancoff approximation (TDA)¹² using the same functional and basis set as for ground state geometry optimization.

Attachment and detachment densities overlap index η_S

Attachment (A) and detachment (D) matrices are obtained from the diagonalization of the difference in the ground and the excited state of interest density matrices.¹³ The eigenvalues correspond to occupation numbers associated to the eigenvectors. The sum over these occupation numbers must be zero, otherwise it would involve a net electron gain or loss of electrons upon the transition. In a next step, the diagonal difference density matrix is split into two matrices, A and D. The attachment and detachment density matrices are built based on the eigenvectors corresponding to positive and negative eigenvalues, respectively.

We can further define a dimensionless η_S index as the overlap between the attachment and detachment densities:¹⁴

$$\eta_S = \frac{1}{\theta} \int dr \sqrt{\rho_D(r) \rho_A(r)}$$
$$\theta = \frac{1}{2} \left[\int dr \sum_{\tau=A,D} \rho_\tau(r) \right]$$

The η_S index takes values ranging from 0 to 1, depending on the charge-transfer character of the electronic transition. The lowest bound value appears when there is strictly no overlap between detachment and attachment densities and correspond to a pure charge transfer (ionic) excitation. The upper bound appears when there is one-to-one overlap of the detachment and attachment densities and correspond to a local excitation.

Zero field splitting calculations

The axial Zero Field Splitting (ZFS) parameter D is related to the interspin distance r as [14]:

$$D = \frac{3}{16} \frac{\mu_0}{h} (g_e \mu_B)^2 \left\langle \frac{1 - 3 \cos^2 \theta}{r^3} \right\rangle$$

With θ the angle between the spin-spin vector and the dipolar Z components defined as the polarization axis. D appears as measure of the degree of charge transfer (CT) character in the triplet excited state. The larger the interspin distance is, the larger the CT character in the triplet excited state is, and the lower the D value.

We have computed the ZFS parameter D for **DPAAnCN** or **CzAnCN** for the T_1 excited state at the DFT level (UKS) using the PBE0 functional and the EPR-II basis set¹⁶ optimized for the computation of hyperfine coupling constants with DFT. We have observed a reduction of D (see Supplementary Table S5) when going from compound 3 to 6, that comes along with a decrease of ΔE_{ST} , confirming the increase in the CT character along the series of the designed compounds.

Table S5: ZFS parameter D, calculated at the PBE0/EPR-II level of theory, for the T_1 excited states of the **DPAAnCN** or **CzAnCN** compounds.

	DPAAnCN	CzAnCN
D (cm ⁻¹)	0.035	0.038
ϕ_s	0.85	0.88

The slightly larger D value for **CzAnCN** compared to **DPAAnCN** is very much in line with the ϕ_s value highlighting the slightly more LE character for T_1 in **CzAnCN**. Interestingly, the ZFS calculations support the trend observed in D parameters magnitudes obtained by fitting the TREPR spectra.

SI-9. Angle-resolved photoluminescence (PL) spectroscopy measurements.

Films of mCP doped with 10% wt of either **DPAAnCN** or **CzAnCN** were deposited on glass substrates by thermal evaporation. The films were encapsulated immediately after deposition and stored in nitrogen atmosphere until measurement (for no longer than 1 day after deposition). Angle-resolved PL measurements were done as reported elsewhere.¹⁵ Briefly, the substrates were optically coupled to a glass hemicylinder using index-matching oil. The samples were excited using a high-power UV LED collimated lamp (ThorLabs). The angle- and spectrally-resolved PL with transverse-magnetic (TM) polarization from the sample was

measured by rotating the stage with the hemicylinder and the sample and collecting the emission from the sample with a fixed optical fiber connected to a spectrometer. A polarizer was inserted in front of the fiber to block transverse-electric polarization which improves the sensitivity of the orientation measurement.

The data was fitted to a transfer-matrix based simulation of the spectral radiant intensity (SRI) of the sample for the different polarizations, using the following equation:

$$I(\lambda, \theta, a) = aI_{TM,v}(\lambda, \theta) + (1 - a)I_{TM,h}(\lambda, \theta).$$

Here, I is the total SRI, $I_{TM,v}$ and $I_{TM,h}$ are the TM components of the SRI emitted by vertical and horizontal dipoles, respectively, λ is the emission wavelength, θ is the collection angle relative to the plane of the film, and a is the anisotropy factor, which is equal to 1 if the emission is entirely from vertical dipoles, equal to 1/3 for isotropically oriented dipoles, and equal to 0 if all of the emissive dipoles are oriented in the plane of the film.

The optical constants required for the optical modelling were measured in-house via variable-angle spectroscopic ellipsometry. Representative plots of the results are shown in Figure S14.

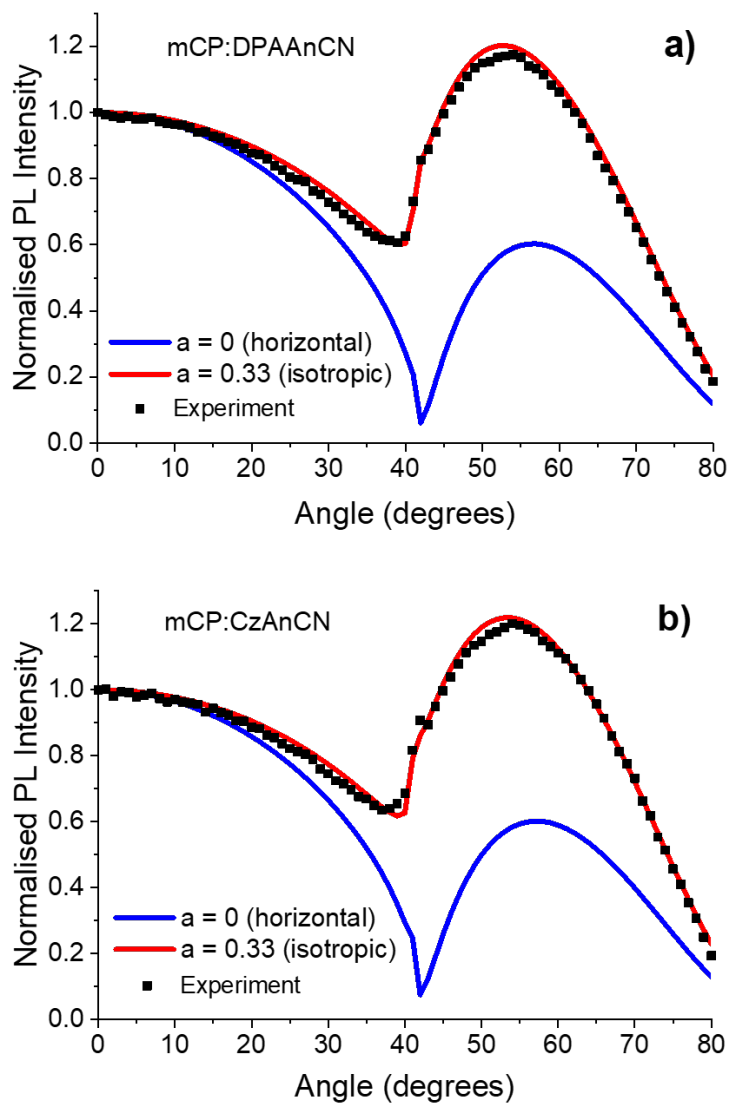


Figure S14. Comparison of experimental (black squares) and simulated angle-resolved PL data of the films mCP:DPAAAnCN (a) and mCP:CzAnCN (b). It can be seen that the best-fitted data corresponds to $a = 0.33$ (isotropic orientation) for both samples.

SI-10. High Resolution Mass Spectrometry (HRMS).

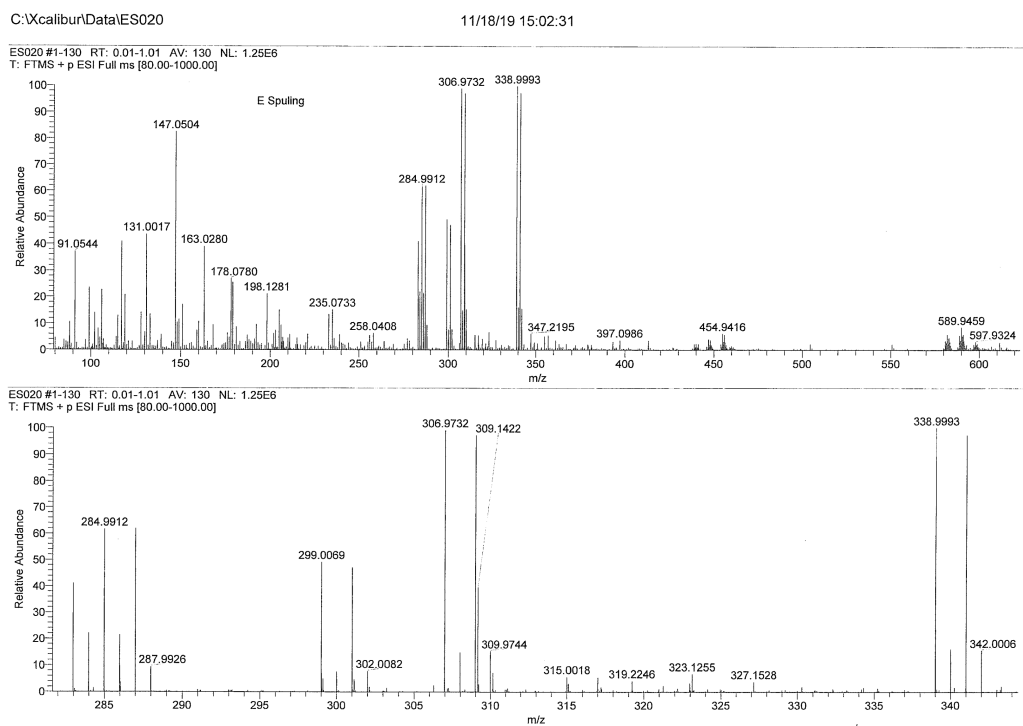


Figure S15. HRMS of 10-bromoanthracene-9-carbaldehyde (4).

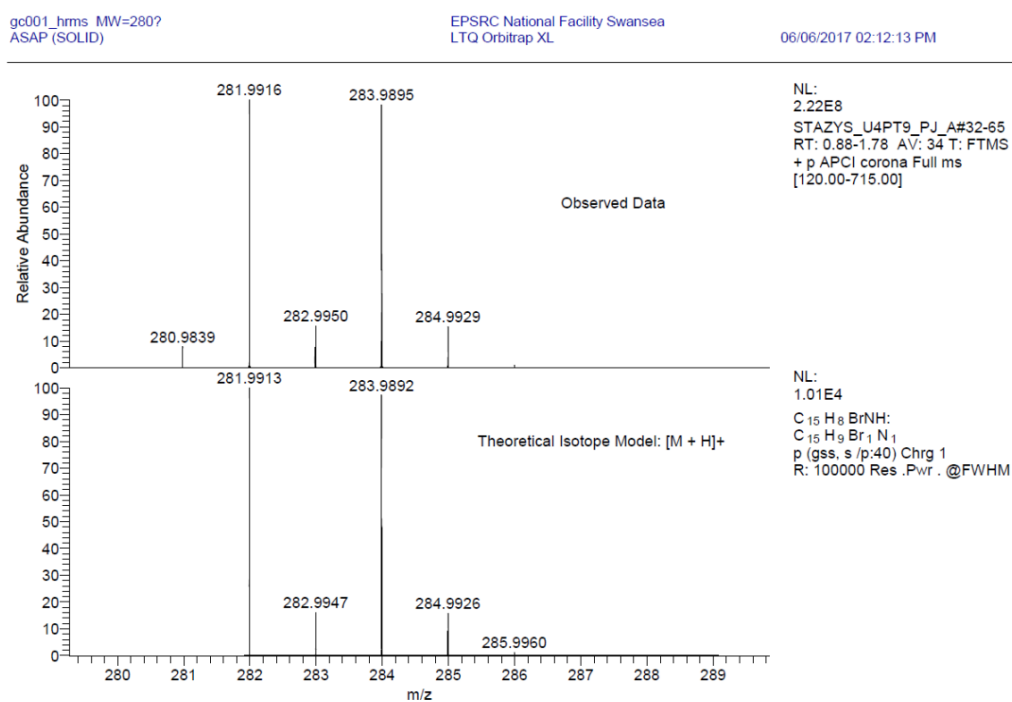


Figure S16. HRMS of 10-bromoanthracene-9-carbonitrile (5).

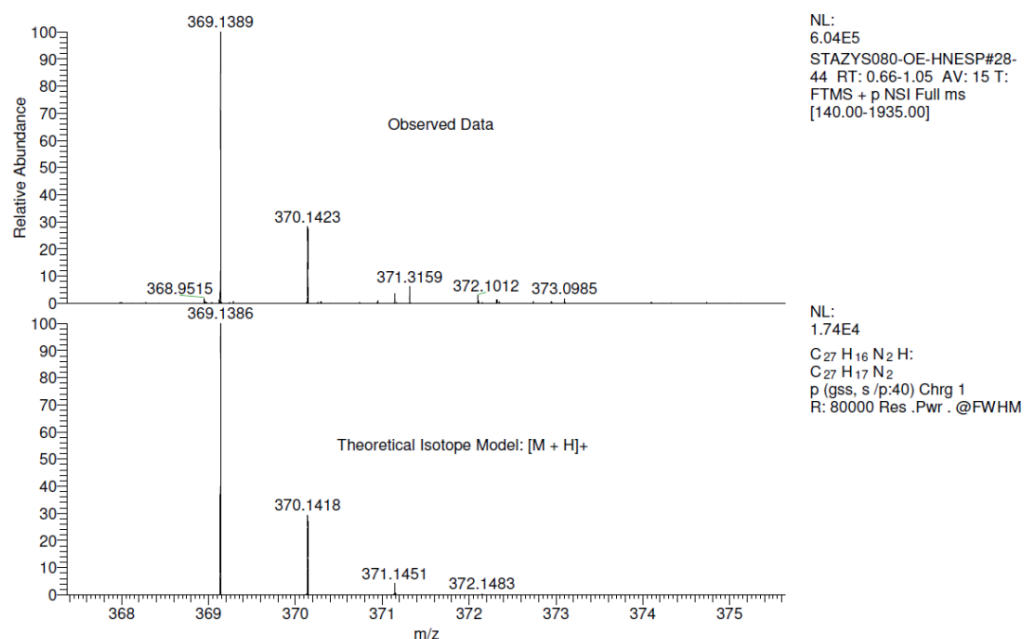


Figure S17. HRMS of C_zAnCN.

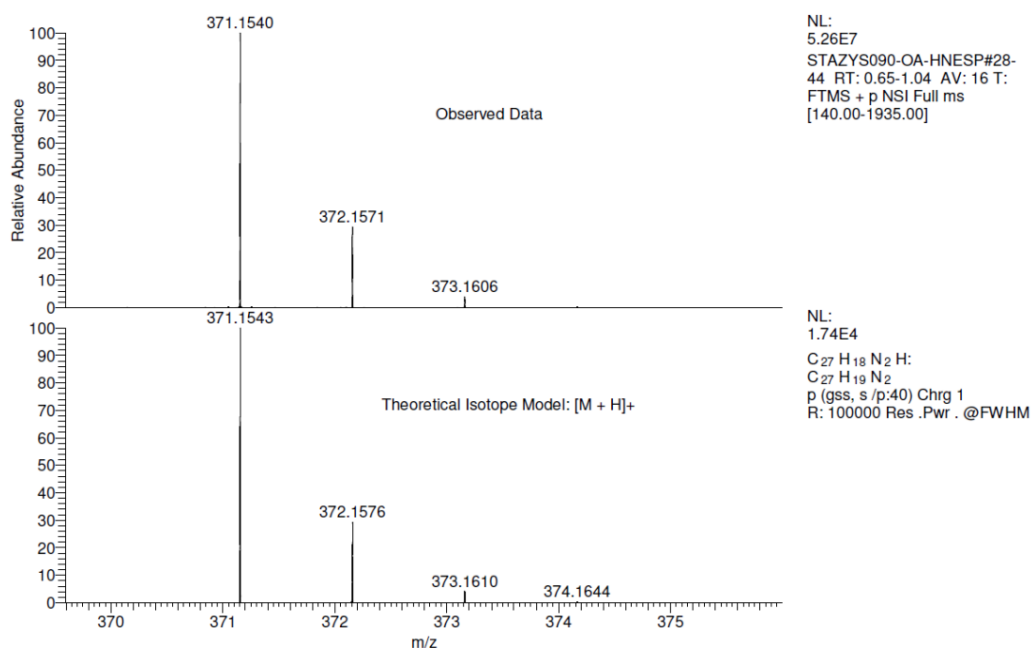


Figure S18. HRMS of DPAAnCN.

SI-11. Elemental Analysis (EA).



Elemental Analysis Service

Please send completed form and samples to:

Stephen Boyer
School of Human Sciences
Science Centre
London Metropolitan University
29 Hornsey Road
London N7 7DD

Telephone: 020 7133 3605
Fax: 020 7133 2577
Email: s.boyer@londonmet.ac.uk

Sample submitted by: Michael Yin Wong	
Address: EZC group, School of Chemistry, University of St Andrews, North Haugh, St Andrews, Fife, KY16 9ST	
Telephone: 01334461754	Email: yw40@st-andrews.ac.uk
Date Submitted: 19-Apr-2015	

Please submit ca. 5 mg of sample.

Sample Reference No.:
Name of Compound: CBZAn
Molecular Formula: C27H16N2
Stability: Air stable
Hazards: none
Other Remarks:

Element	Expected %	Found (1)	Found (2)	
Carbon	88.02	87.90	87.91	
Hydrogen	4.38	4.26	4.30	
Nitrogen	7.60	7.60	7.63	

Authorising Signature:

Date Completed: 29/4/15	Signature:
Comments:	

Figure S19. Elemental analysis report of **CzAnCN**.

Elemental Analysis Service

Please send completed form and samples to:

Stephen Boyer
School of Human Sciences
Science Centre
London Metropolitan University
29 Hornsey Road
London N7 7DD

Telephone: 020 7133 3605
Fax: 020 7133 2577
Email: s.boyer@londonmet.ac.uk

Sample submitted by: Michael Yin Wong	
Address: EZC group, School of Chemistry, University of St Andrews, North Haugh, St Andrews, Fife, KY16 9ST	
Telephone: 01334461754	Email: yw40@st-andrews.ac.uk
Date Submitted: 19-Apr-2015	

Please submit ca. 5 mg of sample.

Sample Reference No.:
Name of Compound: TPAA_n
Molecular Formula: C₂₇H₁₈N₂
Stability: Air stable
Hazards: none
Other Remarks:

Element	Expected %	Found (1)	Found (2)
Carbon	87.54	87.44	87.44
Hydrogen	4.90	5.03	5.11
Nitrogen	7.56	7.45	7.49

Authorising Signature:

Date Completed: 29/04/15	Signature: 
Comments:	

Figure S20. Elemental analysis report of DPAA_nCN.

SI-12. References

- (1). F. de Montigny, G. Argouarch and C. Lapinte, *Synthesis*, 2006, **2006**, 293-298.
- (2). R. H. Goldsmith, J. Vura-Weis, A. M. Scott, S. Borkar, A. Sen, M. A. Ratner and M. R. Wasielewski, *J. Am. Chem. Soc.*, 2008, **130**, 7659-7669.
- (3). G. A. Crosby and J. N. Demas, *J. Phys. Chem.*, 1971, **75**, 991-1024.
- (4). W. H. Melhuish, *J. Phys. Chem.*, 1961, **65**, 229-235.
- (5). V. V. Pavlishchuk and A. W. Addison, *Inorg. Chim. Acta*, 2000, **298**, 97-102.
- (6). *CrystalClear-SM Expert v. 2.1*, Rigaku Americas, The Woodlands, Texas, USA, 2010-2014.
- (7). M. C. Burla, R. Caliandro, M. Camalli, B. Carrozzini, G. L. Cascarano, C. Giacovazzo, M. Mallamo, A. Mazzone, G. Polidori and R. Spagna, *J. Appl. Crystallogr.*, 2012, **45**, 357-361.
- (8). G. Sheldrick, *Acta Crystallogr., Sect. C: Cryst. Struct. Commun.*, 2015, **71**, 3-8.
- (9). *CrystalStructure v4.1* Rigaku Americas, Rigaku Americas, The Woodlands, Texas, USA and Rigaku Corporation, Tokyo, Japan, 2013.
- (10). Z. R. Grabowski, K. Rotkiewicz and W. Rettig, *Chem. Rev.*, 2003, **103**, 3899-4032.
- (11). M. J. Frisch, G. W. Trucks, H. B. Schlegel, G. E. Scuseria, M. A. Robb, J. R. Cheeseman, G. Scalmani, V. Barone, B. Mennucci, G. A. Petersson, H. Nakatsuji, M. Caricato, X. Li, H. P. Hratchian, A. F. Izmaylov, J. Bloino, G. Zheng, J. L. Sonnenberg, M. Hada, M. Ehara, K. Toyota, R. Fukuda, J. Hasegawa, M. Ishida, T. Nakajima, Y. Honda, O. Kitao, H. Nakai, T. Vreven, J. A. Montgomery Jr., J. E. Peralta, F. Ogliaro, M. Bearpark, J. J. Heyd, E. Brothers, K. N. Kudin, V. N. Staroverov, R. Kobayashi, J. Normand, K. Raghavachari, A. Rendell, J. C. Burant, S. S. Iyengar, J. Tomasi, M. Cossi, N. Rega, J. M. Millam, M. Klene, J. E. Knox, J. B. Cross, V. Bakken, C. Adamo, J. Jaramillo, R. Gomperts, R. E. Stratmann, O. Yazyev, A. J. Austin, R. Cammi, C. Pomelli, J. W. Ochterski, R. L. Martin, K. Morokuma, V. G. Zakrzewski, G. A. Voth, P. Salvador, J. J. Dannenberg, S. Dapprich, A. D. Daniels, Ö. Farkas, J. B. Foresman, J. V. Ortiz, J. Cioslowski and D. J. Fox, Gaussian Inc., Wallingford, CT, 2013.
- (12). (a) S. Grimme, *Chem. Phys. Lett.*, 1996, **259**, 128-137; (b) S. Hirata and M. Head-Gordon, *Chem. Phys. Lett.*, 1999, **314**, 291.
- (13). A. Dreuw and M. Head-Gordon, *Chem. Rev.*, 2005, **105**, 4009-4037.
- (14). (a) T. Etienne, X. Assfeld and A. Monari, *J. Chem. Theory Comput.*, 2014, **10**, 3896-3905; (b) T. Etienne, X. Assfeld and A. Monari, *J. Chem. Theory Comput.*, 2014, **10**, 3906-3914.
- (15). (a) A. Graf, P. Liehm, C. Murawski, S. Hofmann, K. Leo and M. C. Gather, *J. Mater. Chem. C*, 2014, **2**, 10298-10304; (b) M. Furno, R. Meerheim, S. Hofmann, B. Lüssem and K. Leo, *Phys. Rev. B*, 2013, **85**, 115205.
- (16). V. Barone, *Recent Advances In Density Functional Methods: (Part I)*, World Scientific, 1995, 287-334.